Seo et al. *NPG Asia Materials* (2021) 13:54
https://doi.org/10.1038/s41427-021-00321-z

NPG Asia Materials

ARTICLE Open Access

Electrical characteristics of amyloid beta peptides in vertical junctions

Sohyeon Seo[1,2], Jinju Lee[1], Jungsue Choi[1], G. Hwan Park[1,3], Yeseul Hong[1,3] and Hyoyoung Lee[1,2,3,4]

Abstract

Assembled amyloid beta (Aβ) peptides have been considered pathological assemblies involved in human brain diseases, and the electron transfer or electron transport characteristics of Aβ are important for the formation of structured assemblies. Here, we report the electrical characteristics of surface-assembled Aβ peptides similar to those observed in Alzheimer's patients. These characteristics correlate to their electron transfer characteristics. Electrical current–voltage plots of Aβ vertical junction devices show the Aβ sequence dependence of the current densities at both Aβ monomers (*mono*-Aβs) and Aβ oligomers (*oli*-Aβs), while Aβ sequence dependence is not clearly observed in the electrical characteristics of Aβ planar field effect transistors (FETs). In particular, surface oligomerization of Aβ peptides drastically decreases the activity of electron transfer, which presents a change in the electron transport pathway in the Aβ vertical junctions. Electron transport at *oli*-Aβ junctions is symmetric (tunneling/tunneling) due to the weak and voltage-independent coupling of the less redox-reactive *oli*-Aβ to the contacts, while that at *mono*-Aβ junctions is asymmetric (hopping/tunneling) due to redox levels of *mono*-Aβ voltage-dependently coupled with contact electrodes. Consequently, through vertical junctions, the sequence- and conformation-dependent electrical characteristics of Aβs can reveal their electron transfer activities.

Introduction

Electron transfer and electron transport processes of proteins are important for understanding and gaining insight into their biological functions such as enzymatic reactions[1,2]. However, it is difficult to predict the mechanism of electron transport in proteins due to the size of the protein containing a number of amino acid residues. In biomolecular junctions composed of target biomolecules incorporated between two electrodes, long-range electron transport processes through biomolecules were found to be strongly influenced by molecular size and coupling effects between molecules and electrodes[3,4]. In addition, junction configurations can directly affect the transport efficiency across molecules with regard to the presence of molecular redox activity[5–7]. For example, junction conductance across proteins is influenced by the electron transport efficiency of interactions between redox-active residues and electrodes[7]. Thus, electron transport behaviors across protein junctions could be involved in structural changes, regardless of whether proteins contain redox-active residues. This behavior is important to consider when studying the mechanical structural changes that cause certain proteins to become toxic.

Amyloid beta (Aβ) peptide molecules are critical components of Alzheimer's disease[8–10]. Concentration- or time-dependent morphological changes that occur as a result of fibrillization via oligomerization of Aβ monomers (*mono*-Aβs) during aggregation have been intensively investigated[11–14]. Moreover, electronic conductance studies of Aβ peptide structures have revealed the importance of structural parameters such as the sequences and assembly conditions of Aβ[15,16]. However, understanding how mechanical pathway-dependent chemical

Correspondence: Sohyeon Seo (sshyeon@skku.edu) or Hyoyoung Lee (hyoyoung@skku.edu)
[1]Department of Chemistry, Sungkyunkwan University (SKKU), Suwon 16419, Republic of Korea
[2]Creative Research Institute (CRI), Sungkyunkwan University (SKKU), Suwon 16419, Republic of Korea
Full list of author information is available at the end of the article

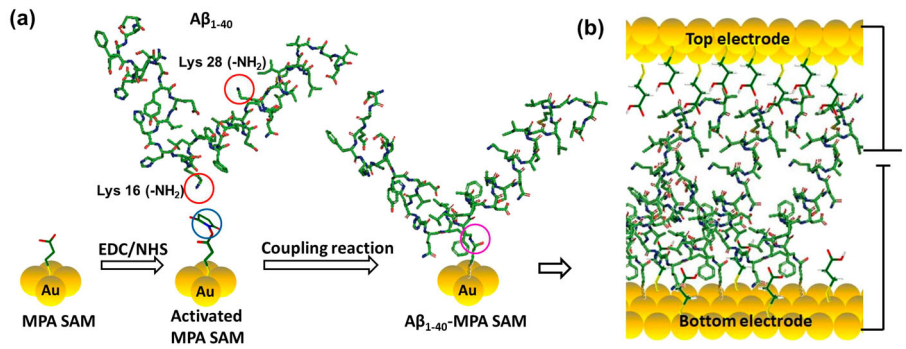

Scheme 1 a The formation of an $A\beta_{1-40}$ molecular layer via a 1-mercaptopropionic acid (MPA) linker monolayer. Terminal carboxylic acid (–COOH) groups of an MPA SAM were activated by EDC/NHS and turned to NHS-ester groups (denoted by a blue circle). The amino group of a lysine residue (Lys 16-NH_2 denoted by a red circle) was coupled with the NHS-ester group to form an amide bond (denoted by a purple circle). **b** The molecular junctions comprised (top)gold−MPA//$A\beta_{1-4}$−MPA−(bottom)gold. The geometric structure of $A\beta_{1-40}$ was obtained from the Protein Data Bank (PDB; 1ba4). *Oli*-Ab_{1-40} was formed by on-surface oligomerization.

activity (or toxicity) results from oligomerization of Aβ remains a significant challenge, although oligomers and fibrils are known to play an active role[17–19]. Based on previous reports[11,15,20], electron transport pathways of amyloid-based proteins whose structural conformation can be determined by a mechanical transition from monomers to oligomers result in changes in chemical activity, such as the redox activity of amino acid residues. Thus, oligomerization of Aβ could induce a change in electron transport across structurally altered Aβ molecules (e.g., Aβ oligomers, *oli*-Aβs) on a surface. The electron transport efficiency of *mono*- and *oli*-Aβs can determine the corresponding mechanical pathways and chemical activities during aggregation processes.

In this work, the electrical characteristics of Aβ peptides were presented to describe the conformational status of the peptides. Surface-immobilized Aβ peptide layers (e.g., Aβ−linker−gold or Aβ−linker/graphene (G)) were used. Electron transport pathways through Aβ were investigated by using three Aβ peptides (e.g., $A\beta_{1-40}$, $A\beta_{1-28}$, and $A\beta_{12-28}$) in vertical gold/biomolecule–gold junctions ("/" denotes physical contact and "−" denotes chemical contact). Electrical characteristics of the vertical junctions showed Aβ sequence dependence, while the current flowing in the field effect transistor (FET) with an Aβ peptide/G channel was weakly dependent on the peptide sequences. In particular, the surface oligomerization of the Aβ peptides drastically changed the electron transfer characteristics by shifting the electrochemical potentials associated with the change in chemical activity. This was clearly revealed in the electrical characteristics of Aβ vertical junctions rather than Aβ/G FETs. (1) Redox-active peptide residues of *mono*-Aβs strongly coupled with the linker monolayer led to asymmetric electron transport characteristics. (2) However, oligomeric Aβ junctions exhibited only symmetric electron transport characteristics due to weak redox activity. These findings indicate that the intermolecular assembly of Aβ peptides results in changes in surface chemical activities (i.e., electron transfer activities), leading to changes in the electron transport pathways.

Results and discussion

To study the electrical characteristics of Aβ peptides through a vertical junction, it is important to have well-defined molecular assembly layers on metal electrodes. However, the formation of molecular layers of proteins or polypeptides might be complicated by a lack of spatial control. Thus, a self-assembled molecular linker monolayer of 1-mercaptopropionic acid (MPA) was used to immobilize Aβ onto a gold electrode, which was activated by coupling reactions with 1-ethyl-3-(3-dimethylamino) propyl carbodiimide/*N*-hydroxysuccinimide (EDC/NHS) (Scheme 1). *Mono*-Aβ−MPA molecular layers were formed via chemical bonding of lysine (Lys 16 or 28 denoted with red circles) residues onto the activated MPA (EDC/NHS−MPA) molecular layer (denoted by a blue circle). Then, the vertical junction of top gold−MPA//Aβ−MPA−bottom gold was fabricated.

Conformation- and sequence-dependent electron transfer of Aβ peptide-immobilized surfaces

Characteristics of in-solution oligomerization

Changes in the molecular conformation and chemical activity (i.e., electron transfer activity) due to the oligomerization of Aβ molecules were verified by circular dichroism (CD) spectroscopy and differential pulse voltammetry (DPV). In Fig. 1a, the CD spectrum of *mono*-$A\beta_{1-40}$ solution showed a characteristic absorption minimum of unstructured monomers at approximately 200 nm[19,21]. In-solution oligomerization under our conditions (1 h incubation) resulted in a shift in the absorption

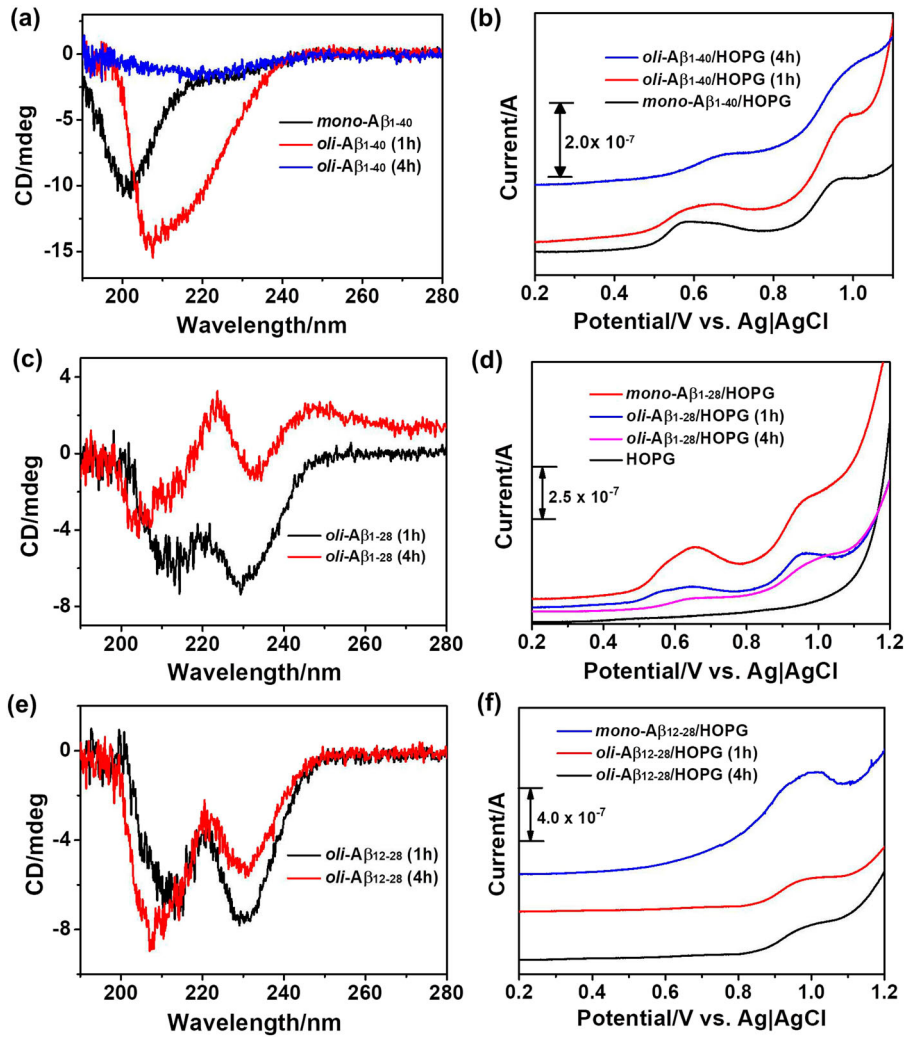

Fig. 1 In-solution oligomerization. a Circular dichroism (CD) spectra of *mono*- and *oli*-Aβ_{1-40} solutions according to the incubation period. **b** Differential pulse voltammograms (DPVs) of *mono*- and *oli*-Aβ_{1-40} physically adsorbed HOPG electrodes. **c** CD spectra of the *oli*-Aβ_{1-28} solution according to the incubation period. **d** DPVs of Aβ_{1-28} physically adsorbed HOPG electrodes. **e** CD spectra of the *oli*-Aβ_{12-28} solution according to the incubation period. **f** DPVs of Aβ_{12-28} physically adsorbed on HOPG electrodes. CD was measured at 25 °C. DPV was measured in 0.1 M phosphate buffer solution at a scan rate of 2 mV s^{-1}.

minimum to approximately 210 nm due to the adoption of a secondary structural conformation[19], indicating oligomeric aggregation of the *mono*-Aβs. After 4 h of incubation, the CD signal was drastically decreased. In addition, CD spectra characterized by two negative peaks for both *oli*-Aβ_{1-28} and *oli*-Aβ_{12-28} also indicated that the *oli*-Aβs had adopted a secondary structural conformation in short Aβ_{1-28} and Aβ_{12-28} peptides (Fig. 1c, e)[19]. The oligomerization effects of *mono*-Aβs on electron transfer behaviors were explored by electrochemical responses of physically immobilized Aβ peptides of *mono*-Aβ and in-solution oligomerized *oli*-Aβ on highly oriented pyrolytic graphite (HOPG) electrodes (Fig. 1b, d, f)[22,23]. The Aβ_{1-40} peptide contains electrochemically active functional groups (e.g., histidine (His 6,13,14), tyrosine (Tyr 10), and methionine (Met 35)) that can be oxidized in the potential range from 0.56 to 0.96 $V_{Ag|AgCl}$ on a glassy carbon (GC) electrode[22,23]. In Fig. 1b, the oxidative peaks of Tyr at approximately 0.56 $V_{Ag|AgCl}$ and His/Met at approximately 1.0 $V_{Ag|AgCl}$ were observed for Aβ_{1-40}; these were also observed at approximately 0.56 $V_{Ag|AgCl}$ for Tyr and approximately 0.96–1.0 $V_{Ag|AgCl}$ for His for Aβ_{1-28} (Fig. 1d), while an oxidative His peak was only observed at approximately 1.0 $V_{Ag|AgCl}$ for Aβ_{12-28} (Fig. 1f). Electrochemically active residues buried by the aggregation of monomers into oligomers can lead to a decrease in electrochemical activity. Thus, the electron transfer sensitivities of electrochemically active residues in the *oli*-Aβs

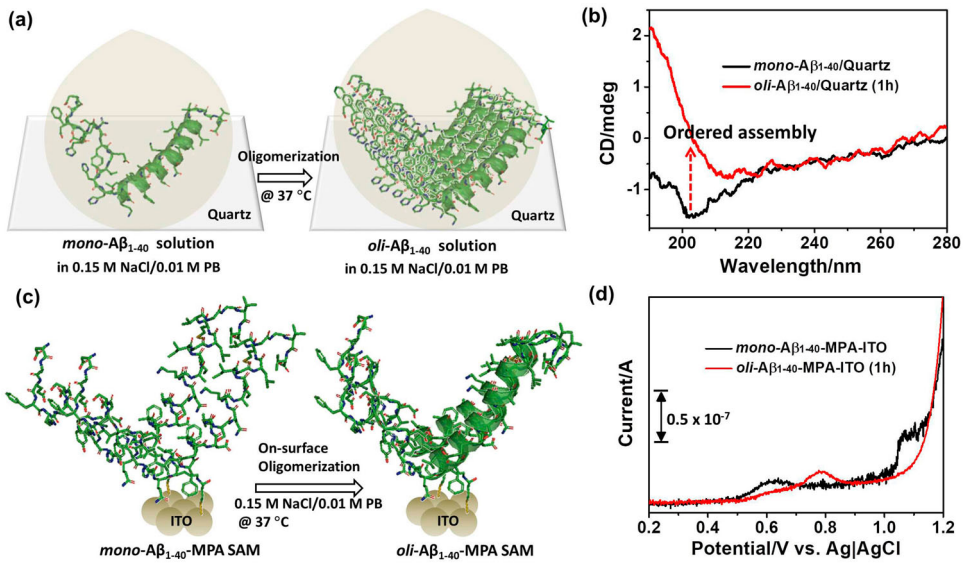

Fig. 2 On-surface oligomerization. a Illustration of on-surface oligomerization of the $A\beta_{1-40}$ molecular layer on a quartz substrate. **b** CD spectra of *mono*- and *oli*-$A\beta_{1-40}$ physically adsorbed on quartz substrates. **c** Illustration of surface oligomerization of the $A\beta_{1-40}$ molecular layer chemically bound on an indium tin oxide (ITO)/glass substrate. **d** DPVs of *mono*- and *oli*-$A\beta_{1-40}$ chemically adsorbed on MPA−ITO/glass in 0.1 M phosphate buffer solution at a scan rate of 2 mV s^{-1}.

were decreased, and the peaks shifted to positive potentials. Furthermore, the process of in-solution Aβ oligomerization (or fibrillization via ordered assembly) was verified by scanning electron microscopy (SEM) (Fig. S1a–d). Apparently, oligomerization of the *mono*-$A\beta_{1-40}$ solution by 1 h incubation could not change the morphology of an *oli*-$A\beta_{1-40}$-deposited surface compared with that of a *mono*-$A\beta_{1-40}$-deposited surface. After 4 and 24 h incubations, short protofibrils and long mature fibrils were observed on the *oli*-$A\beta_{1-40}$-deposited surfaces, respectively.

Characteristics of on-surface oligomerization

To promote the formation of *oli*-Aβ on a substrate, the on-surface oligomerization of *mono*-Aβ was conducted. $A\beta_{1-40}$ molecules oligomerized on a quartz substrate were assembled into *oli*-$A\beta_{1-40}$ and physically adsorbed on the substrate (Fig. 2a) for the identification of structural changes. Unlike the oligomerization of Aβ that occurred in solution, the on-surface oligomerization resulted in a drastic CD spectral change where a pair of positive and negative peaks appeared at approximately 190 and 210 nm, characteristic of a beta-sheet structure[19], indicating the ordered assembly of *oli*-$A\beta_{1-40}$ (Fig. 2b). This indicates the influence of the surface on the oligomerization of Aβ[24]; this surface oligomerization is distinguishable from in-solution oligomerization (Fig. 1). Furthermore, for the formation of *oli*-Aβ molecular layers on an MPA self-assembled monolayer (SAM), the on-surface oligomerization of *mono*-Aβ − MPA molecular layers was conducted in 0.01 M phosphate buffer (PB) solution containing 0.15 M NaCl at 37 °C for 1 h (Scheme 1a and Fig. 2c). *Mono*-Aβ-tethered gold or indium tin oxide (ITO) electrodes were used for electrical and electrochemical measurements, respectively. As shown in Scheme 1a, lysine residues with a charged long chain would be relatively favorable for the coupling reaction with NHS ester compared with the primary amines at the C- or N-termini, which have short chains that can be statically hindered by nearby peptide chains. Unfortunately, CD of the oligomerized amyloid peptide MPA-ITO could not be observed, probably due to insufficient amounts of amyloid peptides on the MPA SAM. In particular, an ITO electrode was suitable for not only the formation of an MPA SAM but also to maintain a stable potential window in PB electrolyte solution. In Fig. 2d, *mono*-Aβ-tethered ITO electrodes ($A\beta_{1-4}$−MPA−ITO) showed a change in electron transfer activities to shift oxidation peaks to approximately 0.6 and 1.05 $V_{Ag|AgCl}$, as shown in Fig. 1. This electrochemical activity changed significantly after the oligomerization on the surface was allowed to proceed for 1 h, whereas physically adsorbed *oli*-Aβs that were oligomerized in solution showed a gradual decrease in electrochemical activity as incubation time increased (Fig. 1b). Only one peak at approximately 0.8 $V_{Ag|AgCl}$ was observed for the *oli*-$A\beta_{1-4}$−MPA−ITO. One of the possible reasons is that electrochemically active residues on the Aβ molecules tethered on the electrodes via chemical binding are probably more hindered by bulky side residues than physically adsorbed Aβ

molecules. Thus, electron transfer from the electrode could be blocked, even at an early stage of oligomerization (e.g., 1 h incubation)[23]. The other possible reason could be a change in electron transfer activity due to the strong interaction with the electrode leading to a change in chemical reaction potentials.

Oligomeric changes in Aβ on the surface induced a change in the surface hydrophilicity (Fig. S2), which can change the electrochemical activity of the surface in the electrolyte. Both MPA and EDS/NHS−MPA SAMs are hydrophilic and can interact positively with hydrophilic residues of *mono*-Aβs. After modification of the SAMs with Aβ molecules, the surfaces retained their hydrophilicity (Fig. S2a). However, oligomerization of *mono*-Aβ SAM led to a decrease in surface hydrophilicity (Fig. S2b). This surface change could result in the electrochemical hindrance of *oli*-Aβ SAMs, leading to the disappearance of electrochemical reactivity. Clean HOPG, on the other hand, exhibited hydrophobicity (Fig. S2c), inducing repulsive interactions with hydrophilic residues of Aβ molecules, which resulted in the hydrophilic surfaces of the physically adsorbed *oli*-Aβ molecules (Fig. S2d). Thus, the electrochemical activity of Aβ molecules in *oli*-Aβs/HOPG was retained for a few hours of incubation, unlike that of the Aβ molecules in *oli*-Aβs−MPA−ITO.

Surface morphology and binding energy of Aβ peptide–MPA monolayers

In molecular electronic devices, the surface order (or roughness) of molecular layers influences the junction properties[25]. To explore changes in surface morphology by *mono*-Aβ modification on an MPA SAM and further on-surface oligomerization, *mono*- or *oli*-$A\beta_{1-40}$ molecular SAMs were examined by scanning tunneling microscopy (STM) (Fig. 3a–c). STM images were used to evaluate the surface morphology in nanoscale molecular layers on a single-crystal electrode. The etch pits formed during thiol adsorption on Au (111) are shown. Surface roughness increased in both *mono*- and *oli*-Aβ molecular layers, indicating that the surface ordering decreased with the formation of Aβ layers compared with that of the MPA layer. Features from defects in the *mono*- or *oli*-Aβ molecular layers were distinguishable from those in the MPA SAM, indicating the formation of new defects in the Aβ layers. The surface morphology of the Aβ molecular layers was slightly changed by oligomerization. These observations indicated that the *oli*-Aβ molecular layers maintained the ordering of *mono*-Aβ molecular layers after oligomerization, which also revealed the advantageous surface conditions of Aβ for the fabrication of molecular layer-based molecular junctions. The microscale surface morphology of different Aβ peptide layers was evaluated by AFM on an e-beam-deposited gold electrode (Fig. S3a–c). The surface roughness was increased by an increase in the molecular length of Aβ peptides. Ellipsometry measurements showed an increase in the film thickness as the molecular length of Aβ peptides increased (Fig. S3d).

Furthermore, the Aβ peptides with the MPA molecular SAM exhibited changes in their binding energies with gold electrodes; these binding energies were verified by ultraviolet photoelectron spectroscopy (UPS) (Fig. 3d,e). Surface modification with the activated-MPA (i.e., (EDS/NHS)−MPA) SAM led to an increase in binding energies with the electrodes compared to the binding energies of the MPA SAM according to the analysis of the secondary electron cutoff (SEC) region (Fig. 3d). This phenomenon was also observed after modification with *mono*-Aβs. No specific correlation between sequences of Aβ peptides and shifts in work function was found in the SEC region (the left plot in Fig. 3e). However, the energy offset between the Fermi level of the gold electrode and the nearest molecular orbital (e.g., highest occupied molecular orbital, HOMO) became larger in the HOMO region as the sequence length increased (the right plot in Fig. 3e). Thus, electron injection barriers from the electrode to the *mono*-Aβ layers decreased from *mono*-$A\beta_{1-40}$ to *mono*-$A\beta_{1-28}$ and *mono*-$A\beta_{12-28}$, which indicates length-dependent electron transport behaviors in those junctions[26]. Moreover, as oligomerization of the Aβ peptides occurred on the surface, the binding energy contributed by chemical contacts became weaker in the SEC region, and the energy offset between the Fermi level of the electrode and the nearest molecular orbital became larger in the HOMO region. Thus, electron transport across the *mono*-Aβ junction can be favored to a greater extent than that across the *oli*-Aβ junction.

Conformation- and sequence-dependent electrical characteristics of Aβ peptides in soil-state devices

Electrical characteristics of Aβ vertical junctions in a cross-bar device

For the fabrication of a cross-bar device, protein stability could be an issue due to nonphysiological environments during the fabrication of molecular junctions, especially contact formation of a top electrode. Soft contacts such as AFM tips[3,27,28], soft materials[6,29], or gold nanowires[7] have therefore been used to study the electron transport mechanisms of proteins. In this work, the vertical junction devices of Aβ were configured into top gold−MPA//Aβ−MPA−bottom gold, where top gold−MPA electrodes were assembled by a soft contact on bottom *mono*- or *oli*-Aβ−MPA−gold electrodes (Fig. S4). In our previous work[30], the electrical characteristics and stability of the vertical molecular junction assembled by soft contact were verified with length-dependent tunneling transport properties for a series of alkanethiol molecules.

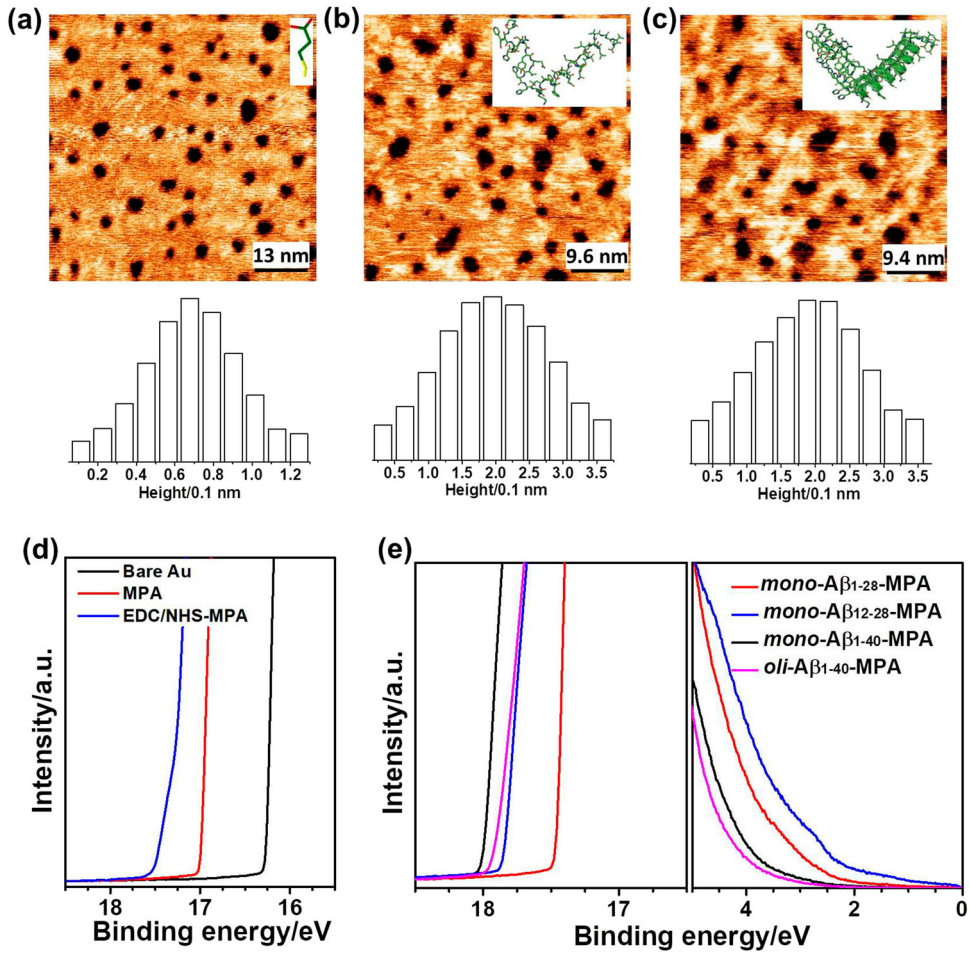

Fig. 3 Changes in surface morphology and binding energy. a–c STM images and histograms of the surface roughness of an MPA SAM, a *mono*-$A\beta_{1-4}$−MPA SAM, and an *oli*-$A\beta_{1-4}$−MPA SAM on Au (111) obtained in 0.1 M $HClO_4$ aqueous solution at $V_{bias} = 0.1\ V_{tip}$, $V_{sub} = 0.1\ V_{SCE}$, and $I_{set} =$ 0.1 nA. **d**, **e** Ultraviolet photoelectron spectroscopy (UPS) spectra of each molecular layer.

Three different peptides ($A\beta_{1-40}$, $A\beta_{1-28}$, and $A\beta_{12-28}$) formed *mono*-Aβ and *oli*-Aβ molecular junctions. Plots of current density against voltage (*J/V)* clearly showed that *mono*-Aβ molecular junctions had asymmetric characteristics (Fig. 4a, b), while *oli*-Aβ junctions had symmetric characteristics (Fig. 4d, e). The statistical *J* curves as a function of applied voltage (with 95% confidence intervals of the mean) were obtained with 50 devices for each SAM. These are molecular junctions of non-shorted devices, which allowed >80% yield. For both *mono*- and *oli*-Aβ junctions, molecular length-dependent *J/V* plots were obtained, indicating that the junction distance of a smaller Aβ peptide is shorter than that of a larger Aβ peptide. Thus, the *J* values of $A\beta_{12-28}$ junctions were larger than those of $A\beta_{1-28}$ and $A\beta_{1-40}$ junctions, as expected. For *mono*-Aβ junctions, the *J/V* rectifications indicated asymmetric electronic coupling via either chemical or physical contacts of Aβ peptides to the electrode, although compositionally symmetric junctions were fabricated for (top) Au−MPA//Aβs −MPA−Au (bottom).

In particular, the asymmetric *J/V* plots were found to be dependent on the bias voltage value. At a low voltage range (±0.5 V), all *mono*-Aβ junctions had symmetric sigmoidal curves (Fig. S5), while in the voltage range higher than ±1.0 V, asymmetric sigmoidal *J/V* curves were observed. This bias voltage-dependent asymmetric electron transport indicates current rectification behavior involving the asymmetric electronic structure of *mono*-Aβ molecules induced by a high bias voltage[31,32]. Furthermore, the *J* values decreased in the oligomeric Aβ junctions of (top) Au−MPA//*oli*-Aβ−MPA−Au (bottom). Thus, oligomerization of Aβ peptides in molecular layers can equalize the electronic and/or contact properties in their molecular junctions.

The effects of the asymmetric contacts were examined by using control devices (Fig. S6). Junctions composed of asymmetric contacts, such as (top) gold−MPA//MPA−gold

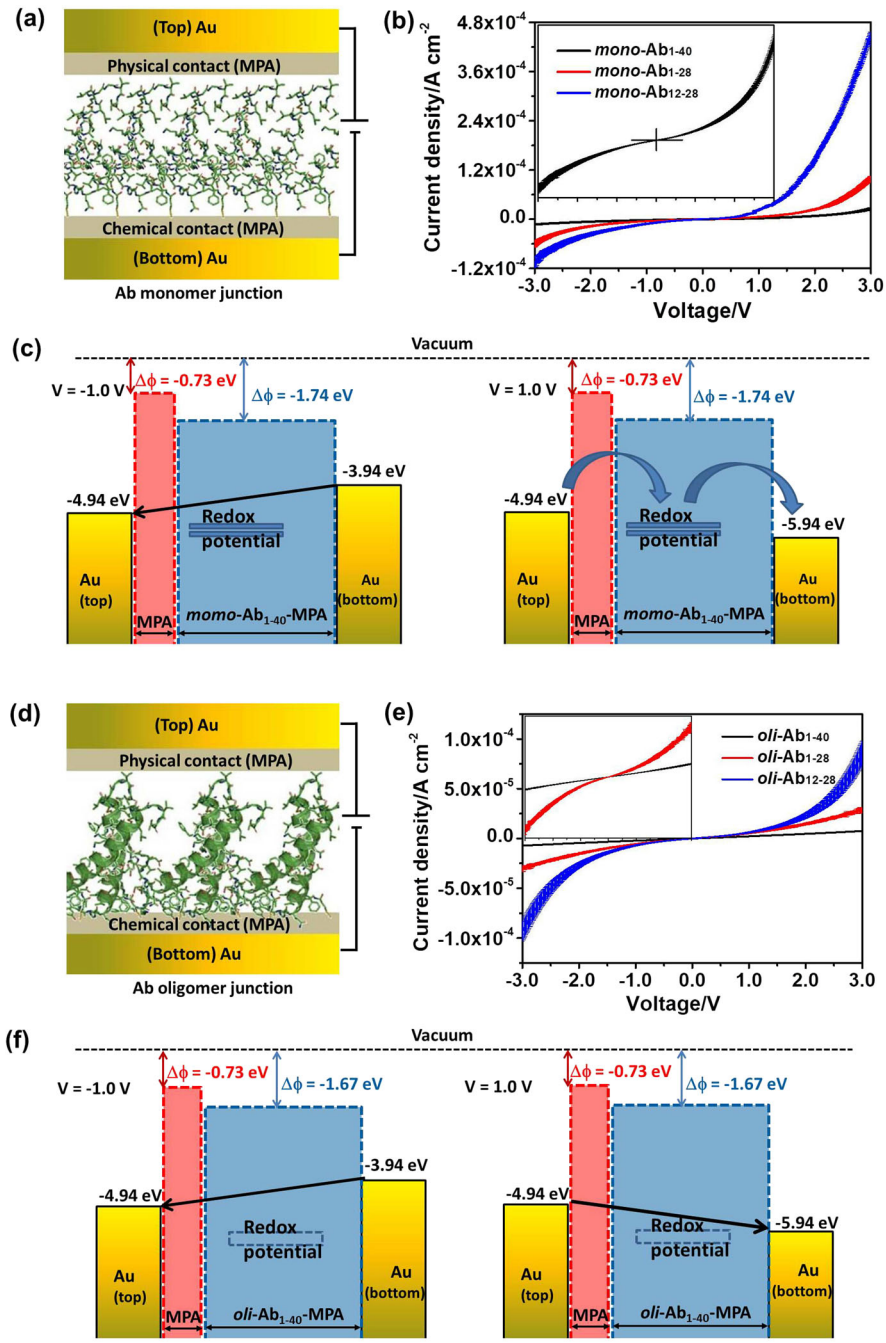

Fig. 4 Electrical characteristics of Aβ peptides in a vertical junction device. a Illustration of a *mono*-Aβ_{1-40} vertical junction. **b** Current density/voltage (*J*/*V*) plots of the Aβ sequence-dependent electron transport characteristics of *mono*-Aβ molecular junctions. Inset: enlarged plots for *mono*-Aβ_{1-40}. The statistical *J* values with 95% confidence intervals of the mean were obtained with 50 devices for each SAM (>80% of device yield). **c** Proposed mechanisms of electron transport through Aβ_{1-40} molecular junctions with regard to applied bias voltages. The straight arrow at $V = -1.0$ V and the curved arrows at $V = 1.0$ V indicate the tunneling (where electrons traverse an energy barrier) and hopping (where electrons traverse localized sites) processes, respectively. The redox levels were obtained from UPS data. **d** Illustration of an *oli*-Aβ_{1-40} vertical junction. **e** Current density/voltage (*J*/*V*) plots of the Aβ sequence-dependent electron transport characteristics of *oli*-Aβ molecular junctions. Inset: enlarged plots for *oli*-Aβ_{1-28} and *oli*-Aβ_{1-40}. The statistical *J* values with 95% confidence intervals of the mean were obtained with 50 devices for each SAM (>80% of device yield). **f** Proposed mechanisms of electron transport through Aβ_{1-40} molecular junctions with regard to applied bias voltages. The straight arrows at $V = -1.0$ and 1.0 V indicate the tunneling processes.

(bottom) and (top) gold//MPA−gold (bottom) junctions without Aβ molecules, were fabricated. These asymmetric contacts exhibited symmetric behavior in the *J/V* curves, similar to *oli*-Aβ molecular junctions, indicating that asymmetric contact junctions do not strongly influence the asymmetric electron transport behavior of *mono*-Aβ molecules. In general, both (exponentially length-dependent) tunneling and (inversely proportional length-dependent) hopping processes can contribute to electron transport pathways across molecular junctions[29,33,34]. Based on the molecular size-dependent *J/V* plots of *mono*-Aβ molecules (Fig. 4b, e), the electron transport mechanism was distance dependent, although junction distances formed by three Aβ molecules could not be correctly determined. In addition, bias voltage-dependent transport characteristics indicated a redox center-involved mechanism[26,35]. The energy level of the redox potential (E_{HOMO}) to vacuum can be estimated by using the formal half-wave potential ($E_{1/2}$)[36]; $E_{HOMO} = E_{abs,NHE} - E_{1/2,NHE}$, where $E_{abs,NHE}$ is the absolute potential energy of the normal hydrogen electrode, NHE ($E_{abs,NHE} = -4.44$ eV and $E_{Ag|AgCl} = 0.197$ E_{NHE}). Thus, the energy levels of the redox potentials of *mono*-$A\beta_{1-40}$ were estimated to be at approximately −5.25 eV and −5.69 eV, whereas that of *oli*-$A\beta_{1-40}$ was measured to be only approximately −5.49 eV (Fig. 2d). In the case of *mono*-$A\beta_{1-40}$, the HOMO energy levels can be arranged between the Fermi levels of gold at 1.0 V, which were depicted at the same location in the junctions in Fig. 4c due to the undefined locations of redox centers. However, one of the HOMO energy levels of *oli*-$A\beta_{1-40}$ can be arranged between the Fermi levels of gold at 1.0 V, which is depicted with a dotted square including the inactive redox center in Fig. 4g.

The energy levels of the oxidation of Aβ residues are likely located between those of the gold electrodes under bias voltages (e.g., 1.0 V), as shown in Fig. 4c, although this does not take into account coupling effects contributed by chemical contacts between the molecular orbitals and the gold electrode. Thus, electron transport can occur in the forward direction ($V = 1.0$ V) via the energy levels of redox-active residues in *mono*-Aβ junctions, suggesting hopping conductance. At the reverse direction ($V = -1.0$ V), the energy levels of redox centers can hardly allow for transporting electrons. In contrast, *oli*-Aβs did not exhibit voltage-dependent transport characteristics, indicating that redox centers are unlikely to be involved in the transport mechanism (Fig. 4f), which was consistent with the electrochemical activity results (Fig. 2d). Nonetheless, the molecular size-dependent *J/V* plots and strong coupling of *mono*- and *oli*-Aβ to the gold electrode via MPA revealed electron tunneling traversing

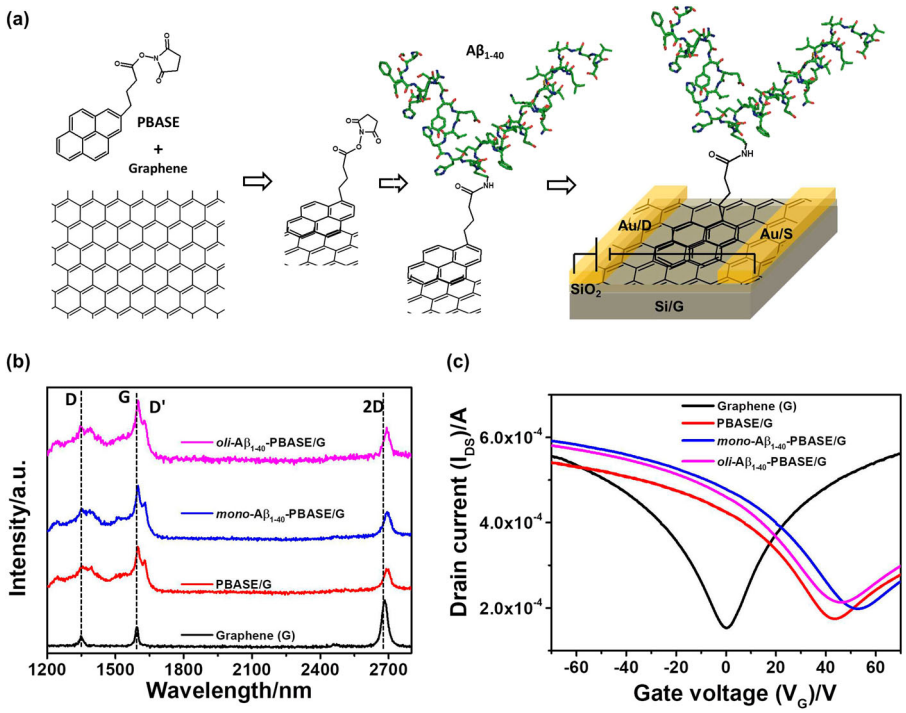

Fig. 5 Electrical characteristics of Aβ peptides in a planar junction device. a Illustration of a *mono*-$A\beta_{1-40}$ − PBASE/graphene channel and an FET device. **b** Raman spectra of each graphene film on SiO_2 substrates. **c** Electrical characteristics of each graphene FET device at $V_{DS} = 0.1$ V.

the energy barriers. Thus, at $V = \pm 1.0$ V, *oli*-Aβs can follow tunneling electron transport, while *mono*-Aβs can follow tunneling electron transport at $V = -1.0$ V and the hopping electron transport at $V = 1.0$ V.

Electrical characteristics of Aβ planar devices: Aβ−PBASE/graphene FETs

Additionally, the electrical characteristics of a *mono*- or *oli*-Aβ assembly in a planar device were explored. The Aβ-immobilized graphene channel was fabricated by using a self-assembled molecular linker monolayer of 1-pyrenebutanoic acid succinimidyl ester (PBASE) (Fig. 5a). Transformation of *mono*-Aβs to *oli*-Aβs was conducted on *mono*-Aβ-immobilized surfaces under the same conditions for the formation of vertical *oli*-Aβ junction devices. In the Raman fingerprint of graphene (Fig. 5b), a sharp and symmetric 2D band at approximately 2682.9 cm^{-1} was clearly observed and shifted to approximately 2695.5 cm^{-1} after modification with PBASE, indicating hole doping on pristine graphene. A D band at approximately 1348.0 cm^{-1} revealing structural defects on graphene appeared for both pristine graphene and PBASE-modified graphene. The G band of pristine graphene shifted from approximately 1595.0 cm^{-1} to approximately 1598.6 cm^{-1}, indicating that the PBASE molecules induce hole doping on pristine graphene. A D′ band appeared at approximately 1630.9 cm^{-1}, indicating another weak disordered feature after modification with PBASE, which is superimposed with one of the peaks[37] of the pyrene structure at 1242.2 cm^{-1}, 1393.7 cm^{-1}, and 1630.9 cm^{-1}. The peak positions of the Raman bands were negligibly changed by further modification with *mono*-Aβs and *oli*-Aβs. The specific influence of *mono*-Aβ sequences was not observed in the peak positions of the Raman spectra (Fig. S7). In addition, the peak ratio of the intensity of the G bands to 2D bands (I_G/I_{2D}) increased with PBASE modification, indicating hole doping[37]. The I_G/I_{2D} ratios increased with *mono*-Aβ−PBASE modification and then decreased again with *oli*-Aβ−PBASE modification.

The hole-doping effect of PBASE and Aβ peptides on graphene was observed in the electrical characteristics of Aβ − PBASE/G-FETs (Figs. 5c and S7c, d). The pyrene linker PBASE on graphene induced a shift of the charge neutrality point to large positive values, indicating the highly concentrated doping of hole carriers. Then, the immobilization of *mono*-Aβs on PBASE/G increased the doping concentration of hole carriers produced by PBASE/G, and the charge neutrality point was positively shifted further. Furthermore, oligomerization of surface-tethered *mono*-Aβ resulted in a negative shift of the charge neutrality point produced by *mono*-Aβ−PBASE/G. These phenomena were noticeably observed at all Aβ−PBASE/G-FETs and were presumably associated with an increase in the surface hydrophobicity (or a decrease in the hydrophilic redox activity) due to the buried redox-active residues. This result was in agreement with the change in the water contact angle after the oligomerization of Aβ. The longer Aβ peptide led to a larger shift in the charge neutrality point by both *mono*- and *oli*-modifications. Unlike *oli*-Aβs in vertical junctions, nonetheless, the electrical characteristics of *oli*-Aβ−PBASE/G-FETs according to peptide sequences were not distinguishable from those of *mono*-Aβ−PBASE/G-FETs. The bottom line shows that both Aβ vertical junctions and Aβ/G FETs (especially $A\beta_{1-40}$) can provide new insights into understanding the electrical characteristics of oligomeric peptides discriminated from those of monomeric peptides, correlating with their electron transfer characteristics.

Conclusion

The electrical characteristics of surface-tethered *mono*- and *oli*-Aβ peptides were investigated. The structural characteristics of the Aβ and the corresponding redox properties were significantly changed by oligomerization on surfaces. The electron transfer of Aβ hardly proceeded after surface oligomerization; this observation was strongly related to a change in the electron transport pathway through Aβ. Different conformations of $A\beta_{1-40}$, $A\beta_{1-28}$, and $A\beta_{12-28}$ were used to explore the electrical characteristics of surface-tethered Aβ peptides in two types of devices (e.g., vertical junction devices and graphene FET devices). In the vertical junction device, the electron transport pathway across the top gold−MPA//*mono*-Aβ−MPA−bottom gold junctions was asymmetric with a strong dependence on the bias voltage. The redox-active peptide residues of the *mono*-Aβs were strongly coupled with the bottom electrode through an MPA monolayer linker, which induced asymmetric coupling of the *mono*-Aβ with gold electrodes at a high voltage (e.g., 1.0 V). This coupling led to electron transport via the energy levels of redox centers through a hopping process. In contrast, the *oli*-Aβ junctions exhibited symmetric characteristics due to reduced redox activity. The less redox-reactive molecular *oli*-Aβ was symmetrically coupled with the electrode contacts, where the energy levels of redox centers were not positioned between the Fermi levels of gold electrodes and the electron transport could follow a tunneling process. However, the current flowing through the FETs with an Aβ−PBASE/G channel was weakly dependent on the peptide sequences and oligomerization. Consequently, investigation of sequence-dependent electron transfer and transport characteristics of Aβ peptides in vertical junctions can predict the chemical activity of ordered aggregates and distinguish the electron transport mechanism of *oli*-Aβ peptides from that of *mono*-Aβ peptides.

Materials and methods

Materials

Amyloid beta (Aβ) 1–40 human (Sigma-Aldrich, USA), [Glu[11]] Aβ 1–28 human (Aldrich, USA), and Aβ 12–28 human (Sigma-Aldrich, USA) were purchased and used directly without further purification. Lyophilized Aβ peptides were stored at −20 °C. For the experiments, peptides were dissolved in 10 mM PB (pH 7.4, purchased from Sigma-Aldrich, USA) containing 1% ammonium hydroxide (NH_4OH) solution (80 μL of 1% NH_4OH solution was used for 1 mg of Aβ peptides) to obtain a final concentration of 25~50 μM Aβ. After vortexing for a few seconds, these solutions were used immediately.

Fabrication of Aβ peptide−MPA SAM−gold (or indium tin oxide)

A SAM of MPA (Sigma-Aldrich) on a pre-cleaned gold/silicon oxide (Au/SiO_2), an Au(111) disc, or indium tin oxide on glass (ITO/glass) electrodes was formed in an ethanol solution containing 2 mM MPA by incubation for 12 h at 4 °C. The MPA SAM was washed thoroughly and dried, and then activated with 1-ethyl-3-(3-dimethylamino) propyl carbodiimide/*N*-hydroxysuccinimide (EDC/NHS) in deionized (DI) water solution containing 10 mM EDC/NHS at 4 °C for 12 h. After washing and drying the (EDC/NHS)−MPA SAMs with ethanol and inert gas, respectively, a 50 μL droplet of each Aβ peptide solution was dropped on the (EDC/NHS)−MPA SAM adsorbed substrates for Aβ modification. These samples were placed into a 50 mL glass vial that was sealed to prevent water evaporation and incubated at 4 °C for 6–12 h. Then, the Aβ−MPA SAMs were washed with PB and DI water and dried with inert gas. To fabricate the *oli*-Aβ−MPA SAMs, a 50 μL droplet of PB solution containing 0.15 M sodium chloride (NaCl, Sigma-Aldrich, USA) was dropped on the Aβ−MPA SAM substrates, and the substrates were placed into a 50 mL glass vial. The vial was sealed to prevent water evaporation and then incubated at 37 °C in an incubator for a predetermined period of time (e.g., 1−4 h). The well-washed and dried *mono*-Aβ−MPA or *oli*-Aβ−MPA samples were stored in a vacuum desiccator in the dark.

Fabrication of Aβ vertical junction devices

A cross-bar device for Aβ vertical junctions was fabricated as reported in previous works[30,35]. Thin-film polydimethylsiloxane (PDMS)-coated polyethylene terephthalate (PET) substrates were used to pattern gold electrodes. PDMS solution was spin-coated on cleaned PET substrates and dried in a vacuum oven at 80 °C overnight. Gold electrodes were patterned on PDMS/PET substrates by electron-beam (e-beam) deposition of gold using a shadow mask at a slow evaporation rate. Au electrode-patterned PDMS substrates were treated with oxygen plasma to become hydrophilic just before chemical modification. The reliability test of the devices was performed by using different alkanethiol SAMs after device fabrication via top//bottom contact assembly (top electrode//molecular SAM–bottom electrode) as described in our previous report[30]. For the device fabrication of Aβ vertical junction devices, a top electrode-patterned substrate modified with an MPA SAM was gently placed onto a bottom electrode-patterned substrate modified with an Aβ−MPA SAM, and the top and bottom electrode arrays were aligned to form vertical junctions (top gold−MPA//Aβ−MPA−bottom gold) (Fig. S3).

Fabrication of Aβ peptide−PBASE/graphene FETs

Graphene (SAINT, Sungkyunkwan University) was grown by chemical vapor deposition (CVD) on Cu foil and transferred onto SiO_2 substrates with patterned gold electrodes by a polymethyl methacrylate (PMMA)-mediated method[38]. The transferred graphene was characterized by Raman spectroscopy with an excitation energy of 532 nm (Ntegra Spectra DUO Max, NT-MDT II). A graphene FET device was immersed in dimethylformamide (DMF) solution containing 10 mM 1-pyrenebutanoic acid succinimidyl ester (PBASE, Aldrich) for the formation of π–π stacked PBASE/graphene (PBASE/G) films at 4 °C for over 7 h. The washed and dried PBASE/G FETs were used for the formation of *mono*-Aβ peptide−PBASE/G and *oli*-Aβ peptide−PBASE/G as described above.

Characterization of molecular assembly and devices

Monomers and oligomers of Aβ peptides were characterized by CD spectrometry (J-1500 CD spectrometer, Jasco, USA). Oligomerization of amyloid beta solution in 0.01 M PB was conducted by adding NaCl to a final concentration of 0.15 M and incubation at 37 °C for various times. For CD measurements of Aβ films, cleaned quartz substrates were used. *Mono*-Aβ film on a quartz substrate was prepared by 6 h incubation at 4 °C after dropping a 50 μL droplet of PB solution containing *mono*-Aβ in a sealed vial. An *oli*-Aβ film on a quartz substrate was prepared by 1 h incubation at 37 °C after dropping a 50 μL droplet of PB solution containing *mono*-Aβ and 0.15 M NaCl in a sealed vial. Then, Aβ samples were washed with PB and DI water and dried with inert gas.

Gold/SiO_2 substrates were used for the morphology and thickness analysis of Aβ films. Morphology and thickness measurements of three monomeric Aβ films were conducted by AFM (SPM 5200, Agilent, USA) and ellipsometry (MG-1000, Nano-View, Korea). Morphological changes as a result of Aβ oligomerization were verified by SEM (JSM-7100F, JEOL, USA). HOPG was used for the electrochemical study of physically adsorbed Aβ films. The first few layers of HOPG were peeled off using tape and then used immediately. For physically adsorbed films of *mono*- or *oli*-Aβs to a certain substrate, a 50 μL droplet

of each solution was dropped on cleaned substrates, which were then placed into a 50 mL glass vial that was then sealed to prevent water evaporation and incubated at 4 °C for 6–12 h. Then, Aβ samples were washed with PB and DI water and dried with inert gas.

Changes in surface binding energy as a result of chemical modification were verified by UPS (AXIS Supra, Kratos, UK). Water contact angle measurements (Phoenix-300, SEO, Korea) were performed for surface characterization of hydrophilicity and hydrophobicity. An Au (111) disc (MaTeck, Germany) was used for STM (SPM 5200, Agilent, USA) studies of Aβ-modified surfaces.

The Au(111) disc was chemically cleaned using piranha solution (a mixture of H_2SO_4 and H_2O_2 at a volume ratio of 3:1), thoroughly washed with DI water, and dried with inert gas. Then, the Au(111) disc was annealed by a hydrogen flame, cooled to room temperature, and immediately further chemically modified. The Aβ-modified Au(111) sample as a working electrode was placed into an electrochemical STM cell composed of a Pt-wire counter electrode and a reference electrode. All electrochemical STM experiments were performed in a degassed aqueous solution containing 0.1 M $HClO_4$ under inert gas.

Electrochemical studies of Aβ molecules were performed by DPV (CHI 620, CH Instruments, USA) using a 5 s pulse period, 0.05 V amplitude, and 0.2 s pulse width. HOPG and ITO/glass electrodes were used for physically adsorbed Aβ layers and chemically adsorbed Aβ layers, respectively. A three-electrode electrochemical cell was used; Pt wire was used as the counter electrode, and an Ag|AgCl (saturated KCl) electrode was used as the reference electrode. The electrolyte was 0.1 M PB solution degassed with an inert gas before use. The geometric area of the working electrodes was 0.2 cm^2.

Current–voltage measurements of the devices were performed under vacuum (~1.0×10^{-3} torr) at room temperature (Keithley 4200-SCS, Tektronix/Keithley, USA).

Acknowledgements
This work was supported by the National Research Foundation of Korea (NRF) grant funded by the Korea Government (MSIT) (NRF-2018R1A2B6006721) and IBS-R011-D1 and partially by a Korea Medical Device Development Fund grant funded by the Korean government (the Ministry of Science and ICT; the Ministry of Trade, Industry and Energy; the Ministry of Health & Welfare; and the Ministry of Food and Drug Safety) (Project Number: KMDF_PR_20200901_0004).

Author details
[1]Department of Chemistry, Sungkyunkwan University (SKKU), Suwon 16419, Republic of Korea. [2]Creative Research Institute (CRI), Sungkyunkwan University (SKKU), Suwon 16419, Republic of Korea. [3]Centre for Integrated Nanostructure Physics (CINAP), Institute of Basic Science (IBS), Suwon 16419, Republic of Korea. [4]Department of Biophysics, Sungkyunkwan University (SKKU), Suwon 16419, Republic of Korea

Competing interests
The authors declare no competing interests.

Supplementary information The online version contains supplementary material available at https://doi.org/10.1038/s41427-021-00321-z.

Received: 20 January 2021 Revised: 12 May 2021 Accepted: 4 June 2021.
Published online: 16 July 2021

References

1. Marcus, R. A. & Sutin, N. Electron transfers in chemistry and biology. *Biochim. Biophys. Acta* **811**, 265–322 (1985).
2. Ron, I. et al. Proteins as electronic materials: electron transport through solid-state protein monolayer junctions. *J. Am. Chem. Soc.* **132**, 4131–4140 (2010).
3. Amdursky, N. et al. Electronic transport via proteins. *Adv. Mater.* **26**, 7142–7161 (2014).
4. Ing, N. L., El-Naggar, M. Y. & Hochbaum, A. I. Going the distance: long-range conductivity in protein and peptide bioelectronic materials. *J. Phys. Chem. B* **122**, 10403–10423 (2018).
5. Venkat, A. S., Corni, S. & Di Felice, R. Electronic coupling between azurin and gold at different protein/substrate orientations. *Small* **3**, 1431–1437 (2007).
6. Castañeda Ocampo, O. E. et al. Mechanism of orientation-dependent asymmetric charge transport in tunneling junctions comprising photosystem I. *J. Am. Chem. Soc.* **137**, 8419–8427 (2015).
7. Fereiro, J. A. et al. Protein electronics: chemical modulation of contacts control energy level alignment in gold-azurin-gold junctions. *J. Am. Chem. Soc.* **140**, 13317–13326 (2018).
8. Hamley, I. W. The amyloid beta peptide: a chemist's perspective. Role in Alzheimer's and fibrillization. *Chem. Rev.* **112**, 5147–5192 (2012).
9. Rauk, A. The chemistry of Alzheimer's disease. *Chem. Soc. Rev.* **38**, 2698–2715 (2009).
10. Chen, G.-f et al. Amyloid beta: Structure, biology and structure-based therapeutic development. *Acta Pharmacol. Sin.* **38**, 1205–1235 (2017).
11. Ahmed, M. et al. Structural conversion of neurotoxic amyloid-β1–42 oligomers to fibrils. *Nat. Struct. Mol. Biol.* **17**, 561–567 (2010).
12. Morel, B., Carrasco, M. P., Jurado, S., Marco, C. & Conejero-Lara, F. Dynamic micellar oligomers of amyloid beta peptides play a crucial role in their aggregation mechanisms. *Phys. Chem. Chem. Phys.* **20**, 20597–20614 (2018).
13. Ono, K., Condron, M. M. & Teplow, D. B. Structure–neurotoxicity relationships of amyloid β-protein oligomers. *Proc. Natl Acad. Sci. USA* **106**, 14745–14750 (2009).
14. Miller, Y., Ma, B. & Nussinov, R. Polymorphism in Alzheimer aβ amyloid organization reflects conformational selection in a rugged energy landscape. *Chem. Rev.* **110**, 4820–4838 (2010).
15. Amit, M., Cheng, G., Hamley, I. W. & Ashkenasy, N. Conductance of amyloid β based peptide filaments: structure–function relations. *Soft Matter* **8**, 8690–8696 (2012).
16. Heo, C. et al. Identifying fibrillization state of aβ protein via near-field thz conductance measurement. *ACS Nano* **14**, 6548–6558 (2020).
17. Lee, S. J. C., Nam, E., Lee, H. J., Savelieff, M. G. & Lim, M. H. Towards an understanding of amyloid-β oligomers: characterization, toxicity mechanisms, and inhibitors. *Chem. Soc. Rev.* **46**, 310–323 (2017).
18. Cohen, S. I. A. et al. Distinct thermodynamic signatures of oligomer generation in the aggregation of the amyloid-β peptide. *Nat. Chem.* **10**, 523–531 (2018).
19. Shea, D. et al. A-sheet secondary structure in amyloid β-peptide drives aggregation and toxicity in alzheimer's disease. *Proc. Natl Acad. Sci. USA* **116**, 8895–8900 (2019).
20. Lindström, F., Bokvist, M., Sparrman, T. & Gröbner, G. Association of amyloid-β peptide with membrane surfaces monitored by solid state nmr. *Phys. Chem. Chem. Phys.* **4**, 5524–5530 (2002).
21. Danielsson, J., Jarvet, J., Damberg, P. & Gräslund, A. The alzheimer β-peptide shows temperature-dependent transitions between left-handed 31-helix, β-strand and random coil secondary structures. *FEBS J.* **272**, 3938–3949 (2005).
22. Enache, T. A. & Oliveira-Brett, A. M. Alzheimer's disease amyloid beta peptides in vitro electrochemical oxidation. *Bioelectrochemistry* **114**, 13–23 (2017).

23. Enache, T. A., Chiorcea-Paquim, A.-M. & Oliveira-Brett, A. M. Amyloid–β peptides time-dependent structural modifications: AFM and voltammetric characterization. *Anal. Chim. Acta* **926**, 36–47 (2016).
24. Moores, B., Drolle, E., Attwood, S. J., Simons, J. & Leonenko, Z. Effect of surfaces on amyloid fibril formation. *PLoS ONE* **6**, e25954–e25954 (2011).
25. Vilan, A., Aswal, D. & Cahen, D. Large-area, ensemble molecular electronics: motivation and challenges. *Chem. Rev.* **117**, 4248–4286 (2017).
26. Wang, Z. et al. Role of redox centre in charge transport investigated by novel self-assembled conjugated polymer molecular junctions. *Nat. Commun.* **6**, 7478 (2015).
27. Ruiz, M. P. et al. Bioengineering a single-protein junction. *J. Am. Chem. Soc.* **139**, 15337–15346 (2017).
28. Zhang, B., Song, W., Brown, J., Nemanich, R. & Lindsay, S. Electronic conductance resonance in non-redox-active proteins. *J. Am. Chem. Soc.* **142**, 6432–6438 (2020).
29. Kumar, K. S., Pasula, R. R., Lim, S. & Nijhuis, C. A. Long-range tunneling processes across ferritin-based junctions. *Adv. Mater.* **28**, 1824–1830 (2016).
30. Seo, S. et al. Nanoparticle linker-controlled molecular wire devices based on double molecular monolayers. *Small* **15**, 1901183 (2019).
31. Yuan, L. et al. Controlling the direction of rectification in a molecular diode. *Nat. Commun.* **6**, 6324 (2015).
32. Nijhuis, C. A., Reus, W. F. & Whitesides, G. M. Mechanism of rectification in tunneling junctions based on molecules with asymmetric potential drops. *J. Am. Chem. Soc.* **132**, 18386–18401 (2010).
33. Marques-Gonzalez, S. & Low, P. Molecular electronics: history and fundamentals. *Aust. J. Chem.* **69**, 244–253 (2016).
34. Lu, Q. et al. From tunneling to hopping: a comprehensive investigation of charge transport mechanism in molecular junctions based on oligo(p-phenylene ethynylene)s. *ACS Nano* **3**, 3861–3868 (2009).
35. Seo, S., Hwang, E., Cho, Y., Lee, J. & Lee, H. Functional molecular junctions derived from double self-assembled monolayers. *Angew. Chem. Int. Ed.* **56**, 12122–12126 (2017).
36. He, J., Fu, Q., Lindsay, S., Ciszek, J. W. & Tour, J. M. Electrochemical origin of voltage-controlled molecular conductance switching. *J. Am. Chem. Soc.* **128**, 14828–14835 (2006).
37. Pantelic, R. S., Fu, W., Schoenenberger, C. & Stahlberg, H. Rendering graphene supports hydrophilic with non-covalent aromatic functionalization for transmission electron microscopy. *Appl. Phys. Lett.* **104**, 134103 (2014).
38. Seo, S., Min, M., Lee, S. M. & Lee, H. Photo-switchable molecular monolayer anchored between highly transparent and flexible graphene electrodes. *Nat. Commun.* **4**, 1920 (2013).